BABAR-CONF-02/003
SLAC-PUB-9169
hep-ex/0203036
March, 2002

Measurement of the B^0 Lifetime with Partial Reconstruction of $\overline{B}^0 \to D^{*+}\rho^-$

The *BABAR* Collaboration

March 27, 2002

Abstract

A sample of about 5500 $\overline{B}^0 \to D^{*+}\rho^-$ and 700 $\overline{B}^0 \to D^{*+}a_1^-$ events is identified, using the technique of partial reconstruction, among 22.7 million $B\overline{B}$ pairs collected by the *BABAR* experiment at the PEP-II storage ring. With these events, the B^0 lifetime is measured to be $1.616 \pm 0.064 \pm 0.075$ ps. As the first time-dependent analysis conducted with partial reconstruction of $\overline{B}^0 \to D^{*+}\rho^-$, this measurement serves as validation for the procedures required to measure $\sin(2\beta + \gamma)$ with this technique.

Presented at the XXXVIIth Rencontres de Moriond on QCD and Hadronic Interactions,
3-16—3/23/2002, Les Arcs, Savoie, France

Stanford Linear Accelerator Center, Stanford University, Stanford, CA 94309

Work supported in part by Department of Energy contract DE-AC03-76SF00515.

The *BABAR* Collaboration,

B. Aubert, D. Boutigny, J.-M. Gaillard, A. Hicheur, Y. Karyotakis, J. P. Lees, P. Robbe, V. Tisserand, A. Zghiche

Laboratoire de Physique des Particules, F-74941 Annecy-le-Vieux, France

A. Palano, A. Pompili

Università di Bari, Dipartimento di Fisica and INFN, I-70126 Bari, Italy

G. P. Chen, J. C. Chen, N. D. Qi, G. Rong, P. Wang, Y. S. Zhu

Institute of High Energy Physics, Beijing 100039, China

G. Eigen, I. Ofte, B. Stugu

University of Bergen, Inst. of Physics, N-5007 Bergen, Norway

G. S. Abrams, A. W. Borgland, A. B. Breon, D. N. Brown, J. Button-Shafer, R. N. Cahn, E. Charles, M. S. Gill, A. V. Gritsan, Y. Groysman, R. G. Jacobsen, R. W. Kadel, J. Kadyk, L. T. Kerth, Yu. G. Kolomensky, J. F. Kral, C. LeClerc, M. E. Levi, G. Lynch, L. M. Mir, P. J. Oddone, M. Pripstein, N. A. Roe, A. Romosan, M. T. Ronan, V. G. Shelkov, A. V. Telnov, W. A. Wenzel

Lawrence Berkeley National Laboratory and University of California, Berkeley, CA 94720, USA

T. J. Harrison, C. M. Hawkes, D. J. Knowles, S. W. O'Neale, R. C. Penny, A. T. Watson, N. K. Watson

University of Birmingham, Birmingham, B15 2TT, United Kingdom

T. Deppermann, K. Goetzen, H. Koch, B. Lewandowski, K. Peters, H. Schmuecker, M. Steinke

Ruhr Universität Bochum, Institut für Experimentalphysik 1, D-44780 Bochum, Germany

N. R. Barlow, W. Bhimji, N. Chevalier, P. J. Clark, W. N. Cottingham, B. Foster, C. Mackay, F. F. Wilson

University of Bristol, Bristol BS8 1TL, United Kingdom

K. Abe, C. Hearty, T. S. Mattison, J. A. McKenna, D. Thiessen

University of British Columbia, Vancouver, BC, Canada V6T 1Z1

S. Jolly, A. K. McKemey

Brunel University, Uxbridge, Middlesex UB8 3PH, United Kingdom

V. E. Blinov, A. D. Bukin, D. A. Bukin, A. R. Buzykaev, V. B. Golubev, V. N. Ivanchenko, A. A. Korol, E. A. Kravchenko, A. P. Onuchin, S. I. Serednyakov, Yu. I. Skovpen, A. N. Yushkov

Budker Institute of Nuclear Physics, Novosibirsk 630090, Russia

D. Best, M. Chao, D. Kirkby, A. J. Lankford, M. Mandelkern, S. McMahon, D. P. Stoker

University of California at Irvine, Irvine, CA 92697, USA

K. Arisaka, C. Buchanan, S. Chun

University of California at Los Angeles, Los Angeles, CA 90024, USA

D. B. MacFarlane, S. Prell, Sh. Rahatlou, G. Raven, V. Sharma

University of California at San Diego, La Jolla, CA 92093, USA

C. Campagnari, B. Dahmes, P. A. Hart, N. Kuznetsova, S. L. Levy, O. Long, A. Lu, M. A. Mazur, J. D. Richman, W. Verkerke

University of California at Santa Barbara, Santa Barbara, CA 93106, USA

J. Beringer, A. M. Eisner, M. Grothe, C. A. Heusch, W. S. Lockman, T. Pulliam, T. Schalk, R. E. Schmitz, B. A. Schumm, A. Seiden, M. Turri, W. Walkowiak, D. C. Williams, M. G. Wilson

University of California at Santa Cruz, Institute for Particle Physics, Santa Cruz, CA 95064, USA

E. Chen, G. P. Dubois-Felsmann, A. Dvoretskii, D. G. Hitlin, S. Metzler, J. Oyang, F. C. Porter, A. Ryd, A. Samuel, S. Yang, R. Y. Zhu

California Institute of Technology, Pasadena, CA 91125, USA

S. Jayatilleke, G. Mancinelli, B. T. Meadows, M. D. Sokoloff

University of Cincinnati, Cincinnati, OH 45221, USA

T. Barillari, P. Bloom, W. T. Ford, U. Nauenberg, A. Olivas, P. Rankin, J. Roy, J. G. Smith, W. C. van Hoek, L. Zhang

University of Colorado, Boulder, CO 80309, USA

J. Blouw, J. L. Harton, M. Krishnamurthy, A. Soffer, W. H. Toki, R. J. Wilson, J. Zhang

Colorado State University, Fort Collins, CO 80523, USA

T. Brandt, J. Brose, T. Colberg, M. Dickopp, R. S. Dubitzky, A. Hauke, E. Maly, R. Müller-Pfefferkorn, S. Otto, K. R. Schubert, R. Schwierz, B. Spaan, L. Wilden

Technische Universität Dresden, Institut für Kern- und Teilchenphysik, D-01062 Dresden, Germany

D. Bernard, G. R. Bonneaud, F. Brochard, J. Cohen-Tanugi, S. Ferrag, S. T'Jampens, Ch. Thiebaux, G. Vasileiadis, M. Verderi

Ecole Polytechnique, LLR, F-91128 Palaiseau, France

A. Anjomshoaa, R. Bernet, A. Khan, D. Lavin, F. Muheim, S. Playfer, J. E. Swain, J. Tinslay

University of Edinburgh, Edinburgh EH9 3JZ, United Kingdom

M. Falbo

Elon University, Elon College, NC 27244-2010, USA

C. Borean, C. Bozzi, L. Piemontese

Università di Ferrara, Dipartimento di Fisica and INFN, I-44100 Ferrara, Italy

E. Treadwell

Florida A&M University, Tallahassee, FL 32307, USA

F. Anulli,[1] R. Baldini-Ferroli, A. Calcaterra, R. de Sangro, D. Falciai, G. Finocchiaro, P. Patteri, I. M. Peruzzi,[2] M. Piccolo, Y. Xie, A. Zallo

Laboratori Nazionali di Frascati dell'INFN, I-00044 Frascati, Italy

S. Bagnasco, A. Buzzo, R. Contri, G. Crosetti, M. Lo Vetere, M. Macri, M. R. Monge, S. Passaggio, F. C. Pastore, C. Patrignani, E. Robutti, A. Santroni, S. Tosi

Università di Genova, Dipartimento di Fisica and INFN, I-16146 Genova, Italy

[1]Also with Università di Perugia, I-06100 Perugia, Italy
[2]Also with Università di Perugia, I-06100 Perugia, Italy

M. Morii

Harvard University, Cambridge, MA 02138, USA

R. Bartoldus, R. Hamilton, U. Mallik

University of Iowa, Iowa City, IA 52242, USA

J. Cochran, H. B. Crawley, J. Lamsa, W. T. Meyer, E. I. Rosenberg, J. Yi

Iowa State University, Ames, IA 50011-3160, USA

G. Grosdidier, A. Höcker, H. M. Lacker, S. Laplace, F. Le Diberder, V. Lepeltier, A. M. Lutz, S. Plaszczynski, M. H. Schune, S. Trincaz-Duvoid, G. Wormser

Laboratoire de l'Accélérateur Linéaire, F-91898 Orsay, France

R. M. Bionta, V. Brigljević , D. J. Lange, M. Mugge, K. van Bibber, D. M. Wright

Lawrence Livermore National Laboratory, Livermore, CA 94550, USA

A. J. Bevan, J. R. Fry, E. Gabathuler, R. Gamet, M. George, M. Kay, D. J. Payne, R. J. Sloane, C. Touramanis

University of Liverpool, Liverpool L69 3BX, United Kingdom

M. L. Aspinwall, D. A. Bowerman, P. D. Dauncey, U. Egede, I. Eschrich, G. W. Morton, J. A. Nash, P. Sanders, D. Smith

University of London, Imperial College, London, SW7 2BW, United Kingdom

J. J. Back, G. Bellodi, P. Dixon, P. F. Harrison, R. J. L. Potter, H. W. Shorthouse, P. Strother, P. B. Vidal

Queen Mary, University of London, E1 4NS, United Kingdom

G. Cowan, S. George, M. G. Green, A. Kurup, C. E. Marker, T. R. McMahon, S. Ricciardi, F. Salvatore, G. Vaitsas

University of London, Royal Holloway and Bedford New College, Egham, Surrey TW20 0EX, United Kingdom

D. Brown, C. L. Davis

University of Louisville, Louisville, KY 40292, USA

J. Allison, R. J. Barlow, J. T. Boyd, A. C. Forti, F. Jackson, G. D. Lafferty, N. Savvas, J. H. Weatherall, J. C. Williams

University of Manchester, Manchester M13 9PL, United Kingdom

A. Farbin, A. Jawahery, V. Lillard, J. Olsen, D. A. Roberts, J. R. Schieck

University of Maryland, College Park, MD 20742, USA

G. Blaylock, C. Dallapiccola, K. T. Flood, S. S. Hertzbach, R. Kofler, V. B. Koptchev, T. B. Moore, H. Staengle, S. Willocq

University of Massachusetts, Amherst, MA 01003, USA

B. Brau, R. Cowan, G. Sciolla, F. Taylor, R. K. Yamamoto

Massachusetts Institute of Technology, Laboratory for Nuclear Science, Cambridge, MA 02139, USA

M. Milek, P. M. Patel

McGill University, Montréal, QC, Canada H3A 2T8

F. Palombo, C. Vite
Università di Milano, Dipartimento di Fisica and INFN, I-20133 Milano, Italy

J. M. Bauer, L. Cremaldi, V. Eschenburg, R. Kroeger, J. Reidy, D. A. Sanders, D. J. Summers
University of Mississippi, University, MS 38677, USA

C. Hast, J. Y. Nief, P. Taras
Université de Montréal, Laboratoire René J. A. Lévesque, Montréal, QC, Canada H3C 3J7

H. Nicholson
Mount Holyoke College, South Hadley, MA 01075, USA

C. Cartaro, N. Cavallo,[3] G. De Nardo, F. Fabozzi, C. Gatto, L. Lista, P. Paolucci, D. Piccolo, C. Sciacca
Università di Napoli Federico II, Dipartimento di Scienze Fisiche and INFN, I-80126, Napoli, Italy

J. M. LoSecco
University of Notre Dame, Notre Dame, IN 46556, USA

J. R. G. Alsmiller, T. A. Gabriel
Oak Ridge National Laboratory, Oak Ridge, TN 37831, USA

J. Brau, R. Frey, E. Grauges , M. Iwasaki, C. T. Potter, N. B. Sinev, D. Strom
University of Oregon, Eugene, OR 97403, USA

F. Colecchia, F. Dal Corso, A. Dorigo, F. Galeazzi, M. Margoni, M. Morandin, M. Posocco, M. Rotondo, F. Simonetto, R. Stroili, E. Torassa, C. Voci
Università di Padova, Dipartimento di Fisica and INFN, I-35131 Padova, Italy

M. Benayoun, H. Briand, J. Chauveau, P. David, Ch. de la Vaissière, L. Del Buono, O. Hamon, Ph. Leruste, J. Ocariz, M. Pivk, L. Roos, J. Stark
Universités Paris VI et VII, Lab de Physique Nucléaire H. E., F-75252 Paris, France

P. F. Manfredi, V. Re, V. Speziali
Università di Pavia, Dipartimento di Elettronica and INFN, I-27100 Pavia, Italy

E. D. Frank, L. Gladney, Q. H. Guo, J. Panetta
University of Pennsylvania, Philadelphia, PA 19104, USA

C. Angelini, G. Batignani, S. Bettarini, M. Bondioli, F. Bucci, E. Campagna, M. Carpinelli, F. Forti, M. A. Giorgi, A. Lusiani, G. Marchiori, F. Martinez-Vidal, M. Morganti, N. Neri, E. Paoloni, M. Rama, G. Rizzo, F. Sandrelli, G. Simi, G. Triggiani, J. Walsh
Università di Pisa, Scuola Normale Superiore and INFN, I-56010 Pisa, Italy

M. Haire, D. Judd, K. Paick, L. Turnbull, D. E. Wagoner
Prairie View A&M University, Prairie View, TX 77446, USA

J. Albert, P. Elmer, C. Lu, V. Miftakov, S. F. Schaffner, A. J. S. Smith, A. Tumanov, E. W. Varnes
Princeton University, Princeton, NJ 08544, USA

[3]Also with Università della Basilicata, I-85100 Potenza, Italy

F. Bellini, G. Cavoto, D. del Re, R. Faccini,[4] F. Ferrarotto, F. Ferroni, M. A. Mazzoni, S. Morganti, G. Piredda, M. Serra, C. Voena

Università di Roma La Sapienza, Dipartimento di Fisica and INFN, I-00185 Roma, Italy

S. Christ, R. Waldi

Universität Rostock, D-18051 Rostock, Germany

T. Adye, N. De Groot, B. Franek, N. I. Geddes, G. P. Gopal, S. M. Xella

Rutherford Appleton Laboratory, Chilton, Didcot, Oxon, OX11 0QX, United Kingdom

R. Aleksan, S. Emery, A. Gaidot, S. F. Ganzhur, P.-F. Giraud, G. Hamel de Monchenault, W. Kozanecki, M. Langer, G. W. London, B. Mayer, B. Serfass, G. Vasseur, Ch. Yèche, M. Zito

DAPNIA, Commissariat à l'Energie Atomique/Saclay, F-91191 Gif-sur-Yvette, France

M. V. Purohit, A. W. Weidemann, F. X. Yumiceva

University of South Carolina, Columbia, SC 29208, USA

I. Adam, D. Aston, N. Berger, A. M. Boyarski, G. Calderini, M. R. Convery, D. P. Coupal, D. Dong, J. Dorfan, W. Dunwoodie, R. C. Field, T. Glanzman, S. J. Gowdy, T. Haas, T. Hadig, V. Halyo, T. Himel, T. Hryn'ova, M. E. Huffer, W. R. Innes, C. P. Jessop, M. H. Kelsey, P. Kim, M. L. Kocian, U. Langenegger, D. W. G. S. Leith, S. Luitz, V. Luth, H. L. Lynch, H. Marsiske, S. Menke, R. Messner, D. R. Muller, C. P. O'Grady, V. E. Ozcan, A. Perazzo, M. Perl, S. Petrak, H. Quinn, B. N. Ratcliff, S. H. Robertson, A. Roodman, A. A. Salnikov, T. Schietinger, R. H. Schindler, J. Schwiening, A. Snyder, A. Soha, S. M. Spanier, J. Stelzer, D. Su, M. K. Sullivan, H. A. Tanaka, J. Va'vra, S. R. Wagner, M. Weaver, A. J. R. Weinstein, W. J. Wisniewski, D. H. Wright, C. C. Young

Stanford Linear Accelerator Center, Stanford, CA 94309, USA

P. R. Burchat, C. H. Cheng, T. I. Meyer, C. Roat

Stanford University, Stanford, CA 94305-4060, USA

R. Henderson

TRIUMF, Vancouver, BC, Canada V6T 2A3

W. Bugg, H. Cohn

University of Tennessee, Knoxville, TN 37996, USA

J. M. Izen, I. Kitayama, X. C. Lou

University of Texas at Dallas, Richardson, TX 75083, USA

F. Bianchi, M. Bona, D. Gamba

Università di Torino, Dipartimento di Fisica Sperimentale and INFN, I-10125 Torino, Italy

L. Bosisio, G. Della Ricca, S. Dittongo, L. Lanceri, P. Poropat, L. Vitale, G. Vuagnin

Università di Trieste, Dipartimento di Fisica and INFN, I-34127 Trieste, Italy

R. S. Panvini

Vanderbilt University, Nashville, TN 37235, USA

[4]Also with University of California at San Diego, La Jolla, CA 92093, USA

C. M. Brown, P. D. Jackson, R. Kowalewski, J. M. Roney
University of Victoria, Victoria, BC, Canada V8W 3P6

H. R. Band, S. Dasu, M. Datta, A. M. Eichenbaum, H. Hu, J. R. Johnson, R. Liu, F. Di Lodovico, Y. Pan, R. Prepost, I. J. Scott, S. J. Sekula, J. H. von Wimmersperg-Toeller, S. L. Wu, Z. Yu
University of Wisconsin, Madison, WI 53706, USA

T. M. B. Kordich, H. Neal
Yale University, New Haven, CT 06511, USA

1 Introduction

The neutral B meson decay modes $B \to D^{*+}h^-$, where h^- is a light hadron (π^-, ρ^-, a_1^-), have been proposed [1] for use in theoretically clean measurements of the Cabibbo-Kobayashi-Maskawa [2] unitarity triangle parameter $\sin(2\beta+\gamma)$. Since the time-dependent CP asymmetries in these modes are expected to be of order 2%, large data samples and multiple decay channels are required for a statistically significant measurement. The low efficiency of reconstructing the D^0 produced in the D^* decay leads to significant loss of signal events. Partial reconstruction of the B meson results in substantially larger efficiency, albeit with higher backgrounds. The overall $\sin(2\beta+\gamma)$ sensitivity is expected to be roughly similar for partial and full reconstruction, and about 90% of the partially reconstructed events cannot be fully reconstructed. Therefore, both full and partial reconstruction can and should be used for the $\sin(2\beta+\gamma)$ measurement.

The measurement of the B^0 lifetime, presented here, constitutes a first step toward measuring $\sin(2\beta+\gamma)$ with partial reconstruction of $\overline{B}^0 \to D^{*+}\rho^-$. In this analysis, we have developed the procedures for candidate reconstruction, background characterization, vertexing, and fitting, all critical components of the time-dependent $\sin(2\beta+\gamma)$ analysis.

2 The *BABAR* Detector and Data Sample

The data used in this analysis were collected with the *BABAR* detector at the PEP-II storage ring. The data consist of 22.7 million $B\overline{B}$ pairs, corresponding to an integrated luminosity of 20.7 fb^{-1} recorded at the $\Upsilon(4S)$ resonance. In addition, 2.6 fb^{-1} were collected about 40 MeV below the resonance. This off-resonance sample is used to study the continuum, $e^+e^- \to q\overline{q}$ background, where $q = \{u, d, s, c\}$.

The *BABAR* detector, described in detail elsewhere [3], consists of five sub-detectors. Surrounding the beam-pipe is a five-layer silicon vertex tracker (SVT), providing precision measurements of the positions of charged particles close to the interaction point and tracking of charged particles with low transverse momentum. Outside the support tube that surrounds the SVT is a 40-layer drift chamber (DCH), filled with an 80:20 helium-isobutane gas mixture. The DCH provides charged particle momentum measurements in a 1.5 T magnetic field, and ionization energy loss measurements that contribute to charged particle identification. Surrounding the DCH is a detector of internally reflected Cherenkov light (DIRC), providing charged particle identification. Outside the DIRC is a CsI(Tl) electromagnetic calorimeter (EMC), used mainly to detect and measure the energy of photons and to provide electron identification. The EMC is surrounded by a superconducting coil, which generates the magnetic field for tracking. Outside the coil, the flux return iron is instrumented with resistive plate chambers, used mainly for muon identification.

PEP-II is an asymmetric energy storage ring, with positron and electron beam energies of about 3.11 and 9.0 GeV. The center-of-mass (CM) frame of the average e^+e^- collision is therefore boosted along the z direction in the lab frame, enabling time-dependent measurements involving reconstruction of B mesons.

3 Analysis Method

3.1 Partial Reconstruction

To partially reconstruct a $\overline{B}^0 \to D^{*+}\rho^-$ candidate[5] , only the ρ and the π_s, the soft pion from the decay $D^{*+} \to D^0\pi_s^+$ decay, are reconstructed. The angle between the momenta of the B and the ρ in the CM frame is then computed:

$$\cos\theta_{B\rho} = \frac{M_{D^{*+}}^2 - M_{B^0}^2 - M_\rho^2 + E_{\rm CM}E_\rho}{2P_B|\vec{p}_\rho|}, \tag{1}$$

where M_x is the mass of particle x, E_ρ and $\vec{p}_\rho$ are the measured CM energy and momentum of the ρ, $E_{\rm CM}$ is the total CM energy of the beams, and $P_B = \sqrt{E_{\rm CM}^2/4 - M_{B^0}^2}$. Given $\cos\theta_{B\rho}$ and the measured four-momenta of the π_s and the ρ, the B four-momentum may be calculated up to an unknown azimuthal angle ϕ around $\vec{p}_\rho$. For every a value of ϕ, the expected D four-momentum, $\mathcal{P}_D(\phi)$, is determined from four-momentum conservation, and the ϕ-dependent "missing mass" is calculated, $m(\phi) \equiv \sqrt{|\mathcal{P}_D(\phi)|^2}$. With $m_{\rm max}$ and $m_{\rm min}$ being the maximum and minimum values of $m(\phi)$ obtained by varying ϕ, we define the missing mass, $m_{\rm miss} \equiv \frac{1}{2}[m_{\rm max} + m_{\rm min}]$. This variable peaks around M_{D^0}, the nominal D^0 mass, for signal events, with a spread of about 3.5 MeV, while background events are more broadly distributed.

We define the D^* helicity angle θ_{D^*} to be the angle between the directions of the D and the B in the D^* rest frame. The value of $\cos\theta_{D^*}$ is computed as in Ref. [4]. The ρ helicity angle θ_ρ is defined as the angle between the directions of the π^0 (from the decay of the ρ) and the CM frame in the ρ rest frame. Since the $\overline{B}^0 \to D^{*+}\rho^-$ decay is $(87.8 \pm 4.5)\%$ longitudinally polarized [5], the $\cos\theta_\rho$ and $\cos\theta_{D^*}$ distributions of signal events peak toward ± 1. Background events have fairly flat distributions, with $B\overline{B}$ background increasing in the region of soft π_s and π^0, making $\cos\theta_{D^*}$ and $\cos\theta_\rho$ useful for background suppression. With knowledge of $\cos\theta_{D^*}$ and $\cos\theta_{B\rho}$, the 3-momentum of the D is determined, up to a two-fold ambiguity and detector resolution effects.

3.2 Event Selection

In order to suppress the continuum background, we select events in which the ratio of the 2nd to the 0th Fox-Wolfram coefficients [6] is smaller than 0.35. Charged ρ candidates are identified by their decay to a "hard" charged pion, π_h, and a π^0. To suppress fake π^0 candidates, the π^0 momentum in the CM frame is required to be greater than 400 MeV. The invariant mass of the π^0 candidate must be within 20 MeV of the nominal π^0 mass. Both the π_h and π_s candidate tracks are required to originate within 1.5 cm of the interaction point in the $x - y$ plane (the plane perpendicular to the beam) and within ± 10 cm of the interaction point along the direction of the beams. Tracks are rejected if their specific ionization and/or Cherenkov angle indicate that they are highly likely to be a kaon or a lepton. The invariant mass $m(\rho)$ of the ρ candidate must be between 0.45 and 1.1 GeV.

The computed cosine of the angle between the B and ρ must satisfy $|\cos\theta_{B\rho}| \leq 1$. To suppress combinatoric background, we require $|\cos\theta_\rho| > 0.3$ and $|\cos\theta_{D^*}| > 0.3$, and reject events in the range $\cos\theta_\rho > 0.3$ and $\cos\theta_{D^*} < -0.3$.

For each $\rho^\pm\pi_s^\mp$ pair that satisfies the above requirements, $m_{\rm miss}$ is calculated. The pair with the smallest value of $|m_{\rm miss} - M_{D^0}|$ in the event is selected, and all others are discarded. Similarly,

[5] Charge conjugate decays are also implied.

the "wrong-sign" $\rho^{\pm}\pi_s^{\pm}$ pair with the smallest $|m_{\rm miss} - M_{D^0}|$ is retained for background studies, as described below. Right-sign events in the range $1.810 < m_{\rm miss} < 1.840$ GeV are classified as sideband events, and are used for background studies. Right- and wrong-sign events satisfying $m_{\rm miss} > 1.845$ GeV are classified as signal region events. All other events are discarded. The efficiency of signal events to satisfy all the signal region criteria is 6.4%.

Events that could be fully reconstructed in the D^0 decay modes $D^0 \to K^-\pi^+$ or $K^-\pi^+\pi^0$ are tagged as fully reconstructed. In addition to satisfying the partial reconstruction criteria above, fully reconstructed events are identified by requiring that the reconstructed D invariant mass be within 40 MeV of M_{D^0}, the difference between the D^* and D invariant masses be between 142 and 150 MeV, the reconstructed CM B energy be within 50 MeV of $E_{\rm CM}/2$, and $m_{\rm ES} > 5.25$ GeV, where $m_{\rm ES} \equiv \sqrt{E_{\rm CM}^2/4 - p_B^2}$ is the beam energy substituted mass and p_B is the reconstructed CM momentum of the B meson.

3.3 Measurement of the Decay Time Difference

The decay position $z_{\rm rec}$ of the partially reconstructed B candidate along the beam direction is determined by constraining the π_h track to originate from the beam-spot in the $x - y$ plane. To account for the B meson flight in the $x - y$ plane, 30 μm are added in quadrature to the beam-spot size. The π_s is not used in this vertex fit in order to simplify the classification of the background, and since its contribution to the vertex precision is small, due to multiple scattering.

The decay position $z_{\rm other}$ of the other B meson along the beam direction, is obtained with all tracks excluding the π_h, the π_s, and any track whose CM angle with respect to either of the two calculated directions of the D is smaller than 1 radian. This "cone cut" reduces $N_{\rm tr}^D$, the number of D daughter tracks used in the other B vertex. The remaining tracks are fit with a constraint to the beam-spot in the $x - y$ plane. The track with the largest contribution to the χ^2 of the vertex, if greater than 6, is removed from the vertex, and the fit is carried out again, until no track fails this requirement.

The decay time difference $\Delta t = (z_{\rm rec} - z_{\rm other})/\gamma\beta c$ is then calculated, where $\gamma\beta$ is the CM frame boost. The value of $\gamma\beta$ is continuously determined from the beam energies, and averages 0.55. The estimated error $\sigma_{\Delta t}$ in the measurement of Δt is calculated from the parameters of the tracks used in the two vertex fits.

Events are rejected if the χ^2 probability of the π_h vertex fit is smaller than 1%, or if the χ^2 probability of the other B vertex is smaller than 0.5%. We also require $|\Delta t| < 15$ ps and $0.3 < \sigma_{\Delta t} < 4$ ps.

The quantities $z_{\rm rec}$ and $z_{\rm other}$ are computed in the same way for fully reconstructed candidates as they are for partially reconstructed candidates. Using the Monte Carlo simulation, it is verified that with the 1 radian cone cut, the $N_{\rm tr}^D$ distribution of events that are fully reconstructed in the mode $D^0 \to K^-\pi^+$ or $K^-\pi^+\pi^0$ is in good agreement with the distribution of partially reconstructed events.

3.4 Backgrounds

The types of events in the partially reconstructed on-resonance sample are classified as follows:

1. Signal: $\overline{B}^0 \to D^{*+}\rho^-$ events, in which the π_h is correctly identified. This requirement ensures that $z_{\rm rec}$ is the decay position of the B meson, up to the effect of detector resolution. The π_s or the π^0 candidates may be mis-reconstructed.

2. $\overline{B}^0 \to D^{*+}a_1^-$: $\overline{B}^0 \to D^{*+}a_1^-$ events, in which the π_h is a daughter of the a_1, and hence originates from the decay point of the B meson.

3. Peaking $B^0\overline{B}^0$ background: $\overline{B}^0 \to D^{*+}\rho^-$ and some $\overline{B}^0 \to D^{*+}a_1^-$ events, in which the π_h originates from the other B meson, resulting in the measurement $\Delta t = 0$, up to the effect of detector resolution and the selection of tracks used in the other B vertex. The $m_{\rm miss}$ distribution of these events peaks around M_{D^0}, similar to signal events.

4. "Combinatoric" $B\overline{B}$ background: Random combinations of π_h, π^0, and π_s candidates, possibly including true ρ decays.

5. $\overline{B} \to D^{**}\rho^-$, where D^{**} stands for a charged or neutral resonance with mass in the range $2.4 - 2.5$ GeV decaying into $D^{*+}\pi$.

6. Continuum, $e^+e^- \to q\overline{q}$ events.

3.5 Probability Density Function

An unbinned maximum likelihood fit is used to obtain the B^0 lifetime τ_{B^0} from the data. The fit is performed simultaneously to on- and off-resonance data, and to on-resonance events which were fully reconstructed. The probability density function (PDF) is a function of Δt, $\sigma_{\Delta t}$, and four "kinematic" variables: 1) $m_{\rm miss}$; 2) $m(\rho)$; 3) $m_{\rm ES}$; and 4) F, a Fisher discriminant that helps distinguish between $B\overline{B}$ and $q\overline{q}$ events. The value of F is computed from the total CM energy flow of tracks and neutral EMC clusters (excluding the ρ and the π_s) into nine volumes, defined by nine 10°-wide concentric cones centered around the ρ CM momentum $\vec{p}_h$. Each cone is folded to combine the energy flow in both hemispheres with respect to $\vec{p}_h$.

The PDF of partially reconstructed on-resonance events is a sum of terms corresponding to the different event types:

$$\begin{aligned}\mathcal{P}(\vec{\xi}) &= f_{\rm signal}\,\mathcal{P}_{\rm signal}(\vec{\xi}) + f_{D^*a_1}\,\mathcal{P}_{D^*a_1}(\vec{\xi}) \\ &+ f_{{\rm peak}B^0}\,\mathcal{P}_{{\rm peak}B^0}(\vec{\xi}) + f_{B\overline{B}}\,\mathcal{P}_{B\overline{B}}(\vec{\xi}) \\ &+ f_{D^{**}}\,\mathcal{P}_{D^{**}}(\vec{\xi}) + f_{q\overline{q}}\,\mathcal{P}_{q\overline{q}}(\vec{\xi}),\end{aligned} \tag{2}$$

where $\vec{\xi} \equiv (m_{\rm miss}, m(\rho), F, \Delta t, \sigma_{\Delta t})$ is the vector of fit variables,

$$\mathcal{P}_i(\vec{\xi}) \equiv \mathcal{M}_i(m_{\rm miss})\,\mathcal{R}_i(m(\rho))\,\mathcal{F}_i(F)\,\mathcal{T}_i(\Delta t, \sigma_{\Delta t}) \tag{3}$$

is the PDF corresponding to event type i, and f_i is the fraction of events of type i in the data sample, where $\sum_i f_i = 1$.

The PDF of the off-resonance sample is $\mathcal{P}_{q\overline{q}}$, which is also used to describe the continuum component of the on-resonance events in Eq. (2).

The PDF of fully reconstructed events is similar to $\mathcal{P}(\vec{\xi})$, except that $\mathcal{F}_i(F)$ is replaced by the function $\mathcal{E}(m_{\rm ES})$. The fractions $f^{\rm f}_{D^*a_1}$, $f^{\rm f}_{{\rm peak}B^0}$, and $f^{\rm f}_{B\overline{B}}$ for this sample are determined from the Monte Carlo simulation, and are of order a few percent. The fractions $f^{\rm f}_{\rm signal}$ and $f^{\rm f}_{q\overline{q}}$ are obtained from a 3-dimensional fit to the $m_{\rm miss}$, $m(\rho)$, and $m_{\rm ES}$ distributions of this sample.

The $m_{\rm miss}$ distribution of signal events is parameterized as a bifurcated Gaussian,

$$\mathcal{M}_{\rm signal}(m_{\rm miss}) \propto \exp\left(-\frac{(m_{\rm miss} - M)^2}{2\sigma^2}\right), \tag{4}$$

where M is the position of the peak, and the value of σ depends on the sign of $m_{\rm miss} - M$. The proportionality constant in this and subsequent PDF expressions is determined by integrating the PDF over the allowed range of the PDF variable. The $m_{\rm miss}$ distributions of the background event types are parameterized as a bifurcated Gaussian plus an ARGUS function [7],

$$\begin{aligned} A(m_{\rm miss}) &\propto m_{\rm miss}\sqrt{1-(m_{\rm miss}/M_A)^2} \\ &\times \exp\left[\epsilon\left(1-(m_{\rm miss}/M_A)^2\right)\right], \end{aligned} \tag{5}$$

where $A(m_{\rm miss}) = 0$ for $m_{\rm miss} > M_A$, and M_A and ϵ are parameters whose values are determined from fits to data or Monte Carlo simulation, as described in Sec. 3.6.

The $\mathcal{R}_i(m(\rho))$ functions are sums of a relativistic P-wave Breit Wigner function and second-order polynomials. The functions $\mathcal{F}_i(F)$ are bifurcated Gaussians, and $\mathcal{E}_i(m_{\rm ES})$ are a Gaussian for signal events and ARGUS functions for the backgrounds.

The Δt PDF of signal events is an exponential decay with the B^0 lifetime, convoluted with a triple-Gaussian resolution function to account for finite detector resolution:

$$\begin{aligned} \mathcal{T}_{\rm signal}(\Delta t, \sigma_{\Delta t}) &= \frac{1}{2\tau_{B^0}} \int d\Delta t_t \; e^{-|\Delta t_t|/\tau_{B^0}} \times \Big[f_n \, G_n(t_r, \sigma_{\Delta t}) \\ &+ f_w \, G_w(t_r, \sigma_{\Delta t}) + f_o \, G_o(t_r, \sigma_{\Delta t}) \Big], \end{aligned} \tag{6}$$

where Δt_t is the true decay time difference between the two B mesons, $t_r \equiv \Delta t - \Delta t_t$ is the Δt residual, G_n, G_w, and G_o are the "narrow", "wide", and "outlier" Gaussians, each of the form

$$G(t_r, \sigma_{\Delta t}) \equiv \frac{1}{\sqrt{2\pi} s \sigma_{\Delta t}} \exp\left(-\frac{(t_r - b)^2}{2(s\sigma_{\Delta t})^2} \right), \tag{7}$$

where s and b are parameters obtained from the fit to data. The coefficients f_i of Eq. (6) satisfy $f_w = 1 - f_n - f_o$. The same Δt PDF parameters are used for signal and $\overline{B}^0 \to D^{*+} a_1^-$ events.

The Δt PDF of the combinatoric $B\overline{B}$ background is

$$\begin{aligned} \mathcal{T}_{B\overline{B}}(\Delta t, \sigma_{\Delta t}) &= \int d\Delta t_t \left[f_\tau \frac{1}{2\tau} \, e^{-|\Delta t_t|/\tau} + (1 - f_\tau) \, \delta(\Delta t_t) \right] \\ &\times \Big[f_n \, G_n(t_r, \sigma_{\Delta t}) + f_w \, G_w(t_r, \sigma_{\Delta t}) \Big], \end{aligned} \tag{8}$$

where $f_w = 1 - f_n$, and the phenomenological parameter τ is different from τ_{B^0} of Eq. (6). The $\delta(\Delta t_t)$ term accounts for events in which the π_h originates from essentially the same point as the tracks dominating the determination of $z_{\rm other}$.

The Δt PDFs of the remaining background types – peaking $B^0\overline{B}^0$, $\overline{B} \to D^{**}\rho^-$, and continuum – are functionally similar to Eq. (8), with small alterations: In $\mathcal{T}_{{\rm peak}B^0}(\Delta t, \sigma_{\Delta t})$, $f_\tau = 0$, reflecting the fact that the π_h originates from the decay of the other B. In $\mathcal{T}_{q\overline{q}}(\Delta t, \sigma_{\Delta t})$, an additional outlier Gaussian is added to Eq. (8). Different parameter values are used for each of the background PDFs.

3.6 Fit Procedure

The B^0 lifetime τ_{B^0} is obtained through a series of fits. First, the kinematic variable PDF parameters of $\overline{B}^0 \to D^{*+} a_1^-$, combinatoric $B\overline{B}$ and the peaking $B^0\overline{B}^0$ background are determined by fitting the

distributions of these variables in the Monte Carlo simulated events. The parameters of $\mathcal{F}_{\rm signal}(F)$, as well as $f_{D^*a_1}$, and $f_{{\rm peak}B^0}$, are also obtained from the Monte Carlo simulation.

The $\mathcal{R}(m(\rho))$, $\mathcal{M}(m_{\rm miss})$, and $\mathcal{E}(m_{\rm ES})$ parameters of signal and continuum events, and the $\mathcal{F}(F)$ parameters of continuum are obtained by fitting the kinematic variable distributions of the data in the signal region. This 4-dimensional fit is performed simultaneously for partially and fully reconstructed on-resonance data, and for off-resonance data. The fractions $f_{q\overline{q}}$ and $f_{B\overline{B}}$ are also determined in this fit, with $f_{\rm signal}$ obtained from $\sum_i f_i = 1$. The value of $f_{D^{**}}$ is set to 0 in this and the subsequent fits, and is later varied when studying systematic errors.

The parameters of $\mathcal{T}_{B\overline{B}}$ are determined by fitting the data in the $m_{\rm miss}$ sideband. The sideband is populated only by combinatoric $B\overline{B}$ and continuum events. Consequently, this fit uses F as the only kinematic variable, and is performed simultaneously for on- and off-resonance data. The parameters of $\mathcal{T}_{q\overline{q}}(\Delta t, \sigma_{\Delta t})$ of this sample are also determined in the fit.

The composition of the wrong-sign event sample in the signal region and the parameters of $\mathcal{T}_{{\rm peak}B^0}(\Delta t, \sigma_{\Delta t})$ are determined from fits to this sample. The parameters of $\mathcal{T}_{q\overline{q}}(\Delta t, \sigma_{\Delta t})$ of this sample are also determined in the fit.

Finally, the signal region parameters of $\mathcal{T}_{\rm signal}(\Delta t, \sigma_{\Delta t})$ and $\mathcal{T}_{q\overline{q}}(\Delta t, \sigma_{\Delta t})$ are determined from a simultaneous fit to the right-sign signal region on-resonance, off-resonance and fully reconstructed data. The parameters of $\mathcal{T}_{B\overline{B}}(\Delta t, \sigma_{\Delta t})$ and $\mathcal{T}_{{\rm peak}B^0}(\Delta t, \sigma_{\Delta t})$ are taken from the sideband and wrong-sign fits, respectively. Use of the sideband and wrong-sign samples for this purpose is validated using the Monte Carlo simulation.

The samples used to obtain parameters of the different Δt PDF components are summarized in Tab. 1.

Table 1: Signal and background Δt PDFs and the data samples from which their parameters are determined. The indicated data samples are used simultaneously in the fits, where "on" and "off" refers to on- and off-resonance data, respectively, and "full" refers to the fully reconstructed event sample.

PDF	Data samples	$m_{\rm miss}$ region	Right/wrong-sign
$\mathcal{T}_{B\overline{B}}(\Delta t, \sigma_{\Delta t})$	on + off	Sideband	Right-sign
$\mathcal{T}_{{\rm peak}B^0}(\Delta t, \sigma_{\Delta t})$	on + off	Signal region	Wrong-sign
$\mathcal{T}_{\rm signal}(\Delta t, \sigma_{\Delta t})$ $\mathcal{T}_{q\overline{q}}(\Delta t, \sigma_{\Delta t})$	on + off + full	Signal region	Right-sign

4 Results

The partially reconstructed signal region on-resonance sample contains 50898 events, including $5266 \pm 251 \pm 34$ $\overline{B}^0 \to D^{*+}\rho^-$ and $691 \pm 36 \pm 4$ $\overline{B}^0 \to D^{*+}a_1^-$ events, as determined by the kinematic variable fit. The systematic errors are due to the finite numbers of events in the Monte Carlo simulation samples used to obtain the kinematic variable distributions of the two $B\overline{B}$ backgrounds and $\overline{B}^0 \to D^{*+}a_1^-$. The fully reconstructed sample contains 255 ± 20 signal events.

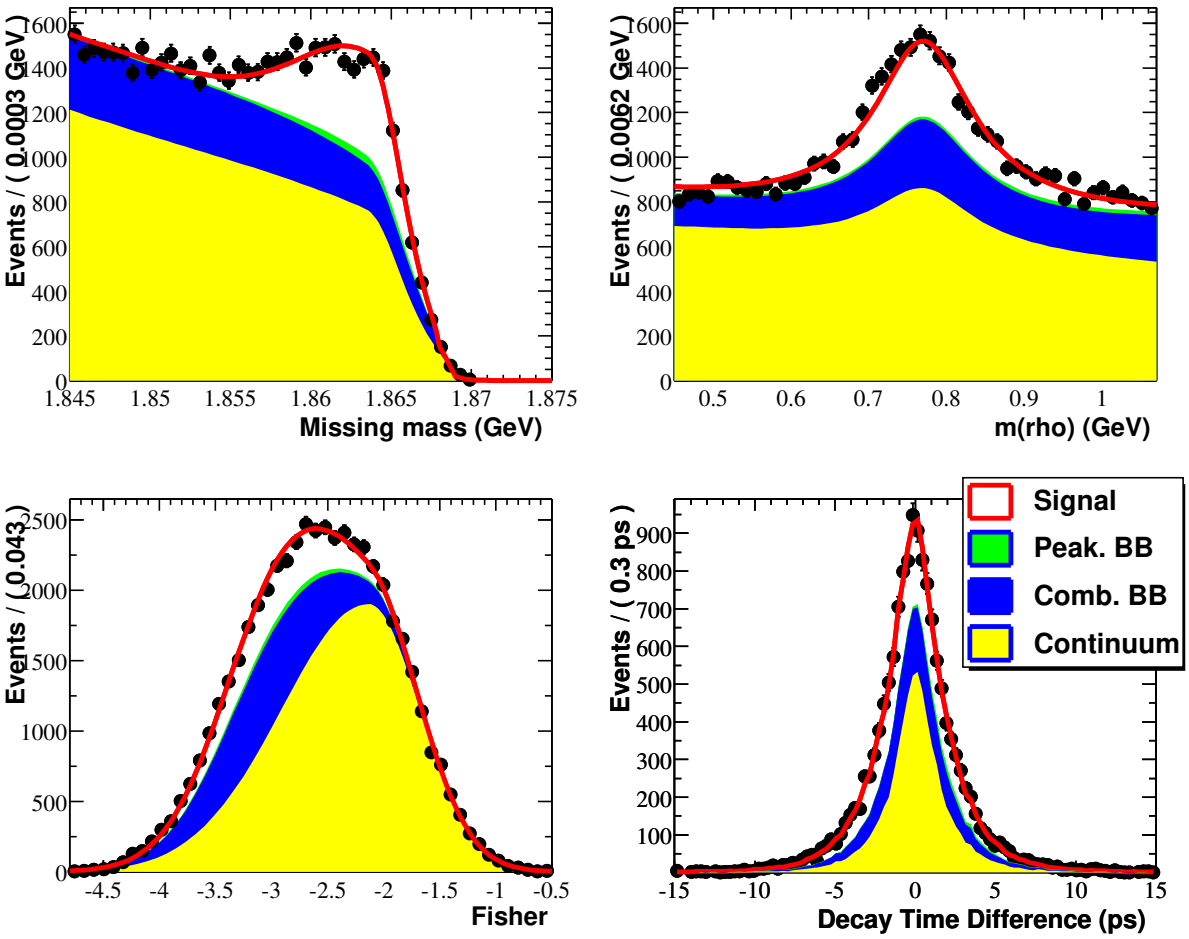

Figure 1: Projections of the PDF of partially reconstructed events onto the on-resonance data in the variables $m_{\rm miss}$ (upper left), $m(\rho)$ (upper right), F (lower left), and Δt (lower right). Events in the Δt projection plot satisfy the additional criteria $m_{\rm miss} > 1.854$ GeV, $0.6 < m(\rho) < 0.93$ GeV, and $F < -2.1$.

Projections of the PDF onto the data are shown in Figs. 1 through 3. The result of the maximum likelihood Δt fit is

$$\tau_{B^0}^{\rm raw} = 1.535 \pm 0.064 \text{ (stat.) } ps, \tag{9}$$

where the error is statistical only.

Several corrections are applied to this result, in order to account for known sources of bias. A correction of $+0.008 \pm 0.011$ ps is due to the assignment of a_1 daughter tracks to the other B vertex, decreasing the measured Δt in $\overline{B}^0 \to D^{*+} a_1^-$ events. The resulting value of 1.543 ps is divided by $R_D = 0.982 \pm 0.022$, the ratio between the B^0 lifetime obtained from a fit to signal Monte Carlo events and the value obtained from a fit to the true Δt_t distribution of this sample. This correction accounts for the effect of D daughter tracks that pass the cone cut and are used in the other B vertex. A correction of $+0.014 \pm 0.013$ ps is applied to this result, to account for a possible bias due to event selection, determined by fitting the true Δt_t distribution of signal events passing the

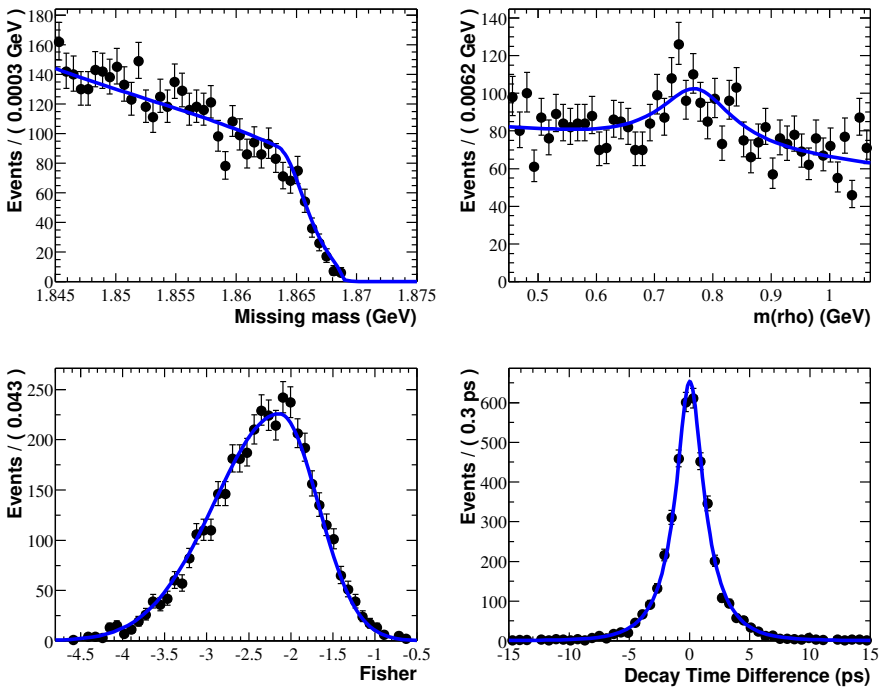

Figure 2: Projections of the PDF of continuum events onto the off-resonance data in the variables $m_{\rm miss}$ (upper left), $m(\rho)$ (upper right), F (lower left), and Δt (lower right).

selection criteria. The magnitudes and errors of all these corrections are obtained from the Monte Carlo simulation.

The fit PDF was used to generate and fit hundreds of Monte Carlo samples, each corresponding to the data sample in number of events and PDF parameters. The value of τ_{B^0} obtained from these fits was on average lower than the generated value by 0.031 ± 0.005 ps. Repeating these studies with different Monte Carlo sample sizes, this bias is understood to be due to limited sample statistics. A correction of this magnitude is therefore added to the value of τ_{B^0}. The fully corrected result is

$$\tau_{B^0} = 1.616 \pm 0.064 \text{ (stat.) ps.} \tag{10}$$

5 Systematic Errors and Cross Checks

Several sources of systematic error are considered. The statistical error matrix obtained from the wrong-sign signal region Δt fit is used to vary the parameters of the peaking $B^0\overline{B}^0$ background, taking into account their correlations. A fit to the right-sign signal region data follows each variation in these background parameters. The resulting variations in τ_{B^0} are added in quadrature to form the total systematic error due to the finite number of events in the wrong-sign sample. With the same procedure, the errors due to the sideband fit are propagated to the wrong-sign signal region and then to the right-sign signal region fits, to obtain the error due to the sideband sample size. The errors due to the finite number of events used in the kinematic variable fits on data and the Monte Carlo simulation are evaluated in the same way.

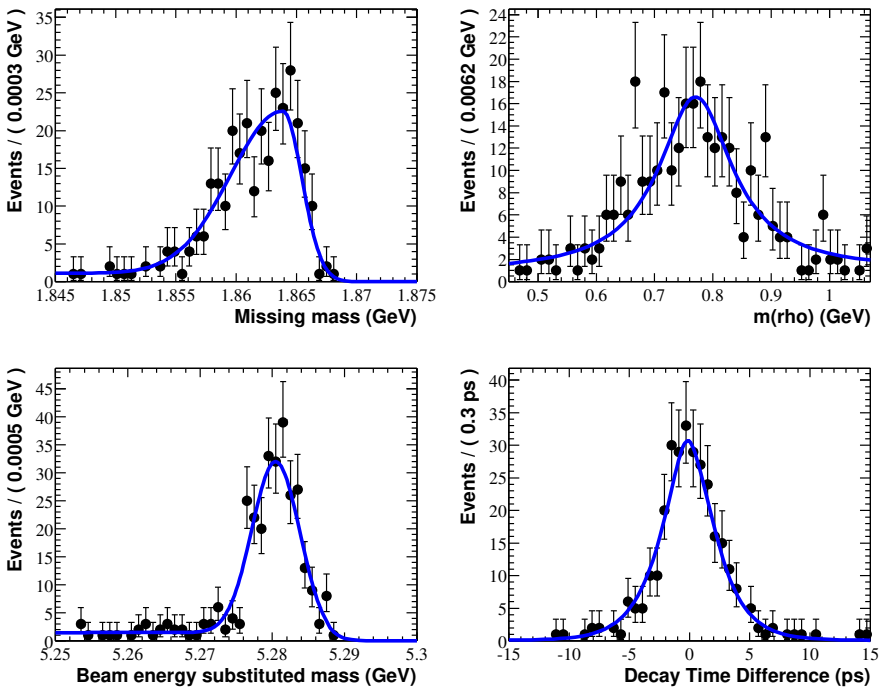

Figure 3: Projections of the PDF of fully reconstructed events onto the fully reconstructed data in the variables $m_{\rm miss}$ (upper left), $m(\rho)$ (upper right), $m_{\rm ES}$ (lower left), and Δt (lower right).

The Monte Carlo statistical errors in the determination of R_D, the $\overline{B}^0 \to D^{*+}a_1^-$ bias, and the selection bias corrections are taken into account. The fraction of events in which D daughter tracks are used in the other B vertex fit is varied by $\pm 5\%$. The magnitude of this variation is determined by comparing the $N_{\rm tr}^D$ distributions of fully reconstructed data and Monte Carlo events. The resulting variation in R_D is used to evaluate the systematic error due to this uncertainty.

The contribution of the $\overline{B} \to D^{**}\rho^-$ background is neglected in the fits. To evaluate the systematic error associated with this, we instead take the number of $\overline{B} \to D^{**}\rho^-$ in the data sample to be 2400, corresponding to $\mathcal{B}(\overline{B} \to D^{**}\rho^-)\ \mathcal{B}(D^{**} \to D^{*+}\pi) = 0.3\%$. This value is estimated from known branching fractions of the decays $\overline{B} \to D^{**}\pi^-$, $\overline{B} \to D^{(*)}\rho^-$, $\overline{B} \to D^{(*)}\pi^-$, and available limits on $\mathcal{B}(\overline{B} \to D^{**}\rho^-)$ [8]. The PDF parameters of this background are taken from the Monte Carlo simulation. Repeating the Δt fit yields a 0.023 ps change in the value of τ_{B^0}, which is taken as the systematic error. The D^{**} states simulated are $D_1(2420)$, $D_2^*(2460)$, and $D_1(j = \frac{1}{2})$, the latter having mass 2.461 GeV and width 290 MeV. No significant difference is found between these states in terms of their effect on the observable quantities of this analysis.

Two variations of the signal Δt PDF are used in fits to the data. In one variation, the parameter b in Eq. (7) is replaced by $b\sigma_{\Delta t}$. In the other, the sum of the narrow and wide Gaussians of Eq. (6) is replaced by a Gaussian convoluted with an exponential. The effect of generating Monte Carlo event samples using one PDF and fitting them using another PDF was studied. Based on these data and Monte Carlo studies, a systematic error of 0.016 ps is estimated due to the choice of signal Δt PDF.

The parameters s and b (Eq. (7)) of the signal and continuum PDF outlier Gaussians are fixed

Table 2: Systematic errors.

Source	Error (ps)
Statistical error of sideband fit	0.033
Statistical error of kinematic fit	0.029
Statistical error of wrong-sign fit	0.002
Monte Carlo statistics: Calculation of R_D	0.036
Monte Carlo statistics: Kinematic parameter fits	0.014
Monte Carlo statistics: Event selection bias	0.013
Monte Carlo statistics: $\overline{B}^0 \to D^{*+}a_1^-$ bias	0.011
$N_{\rm tr}^D$ uncertainty	0.026
Level of $\overline{B} \to D^{**}\rho^-$ background	0.023
Likelihood fit bias	0.016
Variation of fixed parameters	0.015
$Br(\overline{B}^0 \to D^{*+}a_1^-)/Br(\overline{B}^0 \to D^{*+}\rho^-)$	0.005
Level of peaking background	0.003
Bias from fully reconstructed events	0.001
SVT misalignment	0.008
Z-length scale uncertainty	0.007
Beam energies uncertainty	0.002
Total	0.075

in the fit to the right-sign signal region data. To estimate the associated systematic errors, their values are varied within reasonable ranges, and the resulting changes in τ_{B^0} are taken as systematic errors.

Additional systematic errors are due to the uncertainty in the relative branching fractions of $\overline{B}^0 \to D^{*+}a_1^-$ and $\overline{B}^0 \to D^{*+}\rho^-$, the level of peaking background, the introduction of a possible bias due to the use of fully reconstructed events, detector alignment and z-length calibration, and beam energy uncertainty. The total systematic error is 0.075 ps, dominated by the errors due to sideband and kinematic fit statistical errors, and Monte Carlo statistical errors. The systematic errors are listed in Tab. 2.

Several cross-checks were conducted to ensure the validity of the result. The number of signal events detected is in good agreement with the published branching fraction [8] and our signal reconstruction efficiency. The fit was repeated with different values of the cone cut, ranging between 0.6 and 1.2 radians. The data were fitted in bins of the lab frame polar angle, azimuthal angle, and momentum of the π_h, and in sub-samples corresponding to different SVT alignment calibrations. In all cases, no significant variation of the result was observed.

6 Conclusion

In a sample of 22.7 million $B\overline{B}$ pairs, we identified $5521 \pm 252 \pm 34$ $\overline{B}^0 \to D^{*+}\rho^-$ and $691 \pm 36 \pm 4$ $\overline{B}^0 \to D^{*+}a_1^-$ events using partial and full B reconstruction. These events were used to measure

the B^0 lifetime, with the preliminary result being

$$\tau_{B^0} = 1.616 \pm 0.064 \text{ (stat.)} \pm 0.075 \text{ (syst.) ps.} \tag{11}$$

This result is in good agreement with earlier published measurements [8], establishing the validity of the use of partially reconstructed $\overline{B}^0 \to D^{*+}\rho^-$ events in the measurement of $\sin(2\beta + \gamma)$.

We are grateful for the excellent luminosity and machine conditions provided by our PEP-II colleagues, and for the substantial dedicated effort from the computing organizations that support *BABAR*. The collaborating institutions wish to thank SLAC for its support and kind hospitality. This work is supported by DOE and NSF (USA), NSERC (Canada), IHEP (China), CEA and CNRS-IN2P3 (France), BMBF (Germany), INFN (Italy), NFR (Norway), MIST (Russia), and PPARC (United Kingdom). Individuals have received support from the A. P. Sloan Foundation, Research Corporation, and Alexander von Humboldt Foundation.

References

[1] P.F. Harrison and H.R. Quinn (ed.), *BABAR* Physics Book, Chap. 7.6 (1998); R.G. Sachs, Enrico Fermi Institute Report, EFI-85-22 (1985) (unpublished); I. Dunietz and R.G. Sachs, Phys. Rev. **D37**, 3186 (1988) [E: Phys. Rev. **D39**, 3515 (1989)]; I. Dunietz, Phys. Lett. **B427**, 179 (1998).

[2] N. Cabibbo, *Phys. Rev. Lett.* **10**, 531 (1963); M. Kobayashi and T. Maskawa, Prog. Theoret. Phys. **49**, 652 (1973).

[3] The *BABAR* Collaboration, B. Aubert et al., Nucl. Instr. and Methods **A479**, 1 (2002).

[4] The CLEO Collaboration, G. Brandenburg *et al.*, Phys. Rev. Lett. **80**, 2762 (1998).

[5] The CLEO Collaboration, ICHEP98 852, CLEO CONF 98-23 (1998).

[6] G. Fox and S. Wolfram, Phys. Rev. Lett. **41**, 1581 (1978).

[7] The ARGUS Collaboration, H. Albrecht *et al.*, Phys. Lett. **B254**, 288 (1991).

[8] See, for exmaple, The Particle Data Group, C. Caso *et al.*, Review of Particle Physics, Eur. Phys. J. **C15**, 606 (2000).